Structure and burning velocity of turbulent premixed methane/air jet flames in thin-reaction zone and distributed reaction zone regimes

Wang, Zhenkan; Zhou, Bo; Yu, Senbin; Brackmann, Christian; Li, Zhongshan; Richter, Mattias; Aldén, Marcus; Bai, Xue Song

Published in:
Proceedings of the Combustion Institute

DOI:
10.1016/j.proci.2018.09.023

2019

Document Version:
Peer reviewed version (aka post-print)

Structure and burning velocity of turbulent premixed methane/air jet flames in thin-reaction zone and distributed reaction zone regimes

Zhenkan Wang[1], Bo Zhou[1], Senbin Yu[2], Christian Brackmann[1],
Zhongshan Li[1], Mattias Richter[1], Marcus Aldén[1], Xue-Song Bai[2*]

[1]Division of Combustion Physics, Lund University, P.O. Box 11, S221 00 Lund, Sweden
[2]Division of Fluid Mechanics, Lund University, P.O. Box 11, S221 00 Lund, Sweden

Corresponding author:
Xue-Song Bai
Division of Fluid Mechanics, Lund University, P.O. Box 11, S221 00 Lund, Sweden
xue-song.bai@energy.lth.se

Abstract

A series of turbulent premixed methane/air jet flames are studied using simultaneous planar laser diagnostic imaging of OH/CH/temperature and CH/OH/CH_2O. The Karlovitz number of the flames ranges from 25 to 1500, and the turbulence intensity ranges from 16 to 200. These flames can be classified as highly turbulent flames in the thin reactions zone (TRZ) regime and distributed reaction zone (DRZ) regime. The aims of this study are to investigate the structural change of the preheat zone and the reaction zone as the Karlovitz number and turbulent intensity increase, to study the impact of the structural change of the flame on the propagation speed of the flame, and to evaluate the turbulent burning velocity computed in different layers in the preheat zone and reaction zone. It is found that for all investigated flames the preheat zone characterized with planar laser-induced fluorescence (PLIF) of CH_2O is broadened by turbulent eddies. The thickness of the preheat zone increases with the turbulent intensity and it can be on the order of the turbulent integral length at high Karlovitz numbers. The reaction zone characterized using the overlapping layer of OH and CH_2O PLIF signals is not significantly broadened by turbulence eddies; however, the CH PLIF layer is found to be broadened significantly by turbulence. The turbulent burning velocity is shown to monotonically increase with turbulent intensity and Karlovitz number. The increase in turbulent burning velocity is mainly due to the enhanced turbulent heat and mass transfer in various layers of the flame, while the contribution of flame front wrinkling to the turbulent burning velocity is rather minor.

Keywords: planar laser-induced fluorescence; distributed reaction zone regime; turbulent flame speed; flame structures

1. Introduction

Flames in practical combustion devices are often highly turbulent, which, within the context of the regime diagram [1], typically falls into the thin reaction zone (TRZ) regime and the distributed reaction zone (DRZ) regime. In the TRZ regime, the small turbulence eddies can enter and consequently broaden the preheat zone of the flame while the reaction zone is not influenced and remains as a thin layer [2-4]. In contrast, flames in the DRZ regime are hypothetically characterized as reactions taking place volumetrically (i.e. distributed reactions) due to the small-eddy penetration into the reaction zone, a scenario being fundamentally different from the thin flamelet-like reaction zones in the TRZ regime. Due to the distributed reactions, the combustion processes in the DRZ regime may proceed with a relatively uniform temperature distribution and a reduced maximum temperature, which can be a merit for, e.g., NO_x reduction in practical combustion devices.

Experimental studies of distributed reactions in turbulent flames are relatively rare, which is partly due to the difficulties in realization of distributed reactions in laboratory flames and the limitations in diagnostic methods available. There is also no common consensus regarding experimental quantification of the reaction zones. PLIF of HCO may be used to denote the reaction zone since HCO is the product of the OH and CH_2O reaction that contributes to the heat release [3]. As HCO PLIF is often difficult to obtain, the overlapping region of OH radicals and CH_2O, obtained from simultaneous planar laser-induced fluorescence (PLIF) of OH and CH_2O, may be used to denote the heat release zone [5]. Driscoll [4] suggested that the distributed reaction zone regime might be characterized using PLIF of CH radicals. This is because CH radicals are short-lived, which prohibits it being transported an appreciable distance from where it is produced, and its presence in space should therefore be attributed to the formation reactions locally. Very recently, a number of

experiments using PLIF of CH or HCO have been carried out for high speed turbulent premixed jet flames [6-12]. In the experimental study of pilot flame stabilized methane/air jet flames, Zhou et al. [11] showed that with Karlovitz number (Ka) greater than 100, significant spread of CH-PLIF signals could be observed, where Ka is the ratio between the chemical time scale and the Kolmogorov time scale. While this critical Ka of CH broadening coincides very well with the hypothetical boundary of DRZ/TRZ regimes [1], it is however not always the case in other flames. In the experimental study of Wabel et al. [6-9] of methane/air jet flames with a large jet diameter and a lower jet velocity than that of Zhou et al. [10,11], no significant broadening of CH PLIF signal could be observed at high Ka numbers. Therefore, there is a need to perform further investigations under high Ka conditions.

Apart from the structural change of the reaction layers, the propagation of high Ka flames has caused the attention of many research groups. The propagation of turbulent premixed flames, quantified frequently by the turbulent burning velocity (S_T), depends on the flame configuration and the regime of the flame [13-15]. In the flamelet regimes, the Damköhler's hypothesis [14] suggests that S_T is proportional to the flame surface area due to wrinkling, which has been evidenced in both experiments [15] and direct numerical simulation (DNS) studies [16,17]. In the TRZ regime, S_T is however affected by both the increased wrinkling and the enhanced heat and mass diffusion in the broadened preheat zone. In the DRZ regime, in addition to the flame wrinkling and the enhanced heat and mass transfer in the preheat zone, the broadening of the reaction zone may also affect the turbulent burning velocity. At extremely high Ka, S_T may even decrease with increasing turbulent velocity, u' [1,13]. It is useful to correlate S_T with key turbulent parameters such as the turbulent intensity; however, the results have been controversial since S_T is rather sensitive to experiment

devices and evaluation methods [4,13]. In this study, S_T under a large range of flame conditions is computed using different methods and correlation of S_T with the structural changes of flames at TRZ and DRZ regimes is examined.

2. Experiment setup and apparatus

The experimental system employed is shown in Fig. 1a. In the present study, flame structures were visualized using simultaneous laser-diagnostic imaging of temperature/CH/OH with an imaging size of ~23×23 mm^2 to allow for directly correlating the temperature with the reaction zone marker CH. Additionally, simultaneous measurements of OH and CH_2O were also performed with a larger imaging size of ~55×55 mm^2 to allow for analysis of global flame quantities. Snap-shot images of CH, OH, and CH_2O and temperature were acquired through PLIF and Rayleigh Scattering Thermometry (RST, details are referred to Ref. [10]), respectively, following the excitation-detection strategies described in our previous work [10]. High imaging quality and signal fidelity for each measured scalar has been ensured [10,11]. For all scalars measured, the camera gates were set to less than 50 ns and proper optical filters (cf. [10] for details) were employed for background rejection. For the PLIF measurements, the signal-to-background-noise ratio (SBNR) was defined as the ratio between the mean of the signal and the standard deviation of the background noise, which was estimated to be better than 17 for CH-PLIF and 32 for OH-PLIF under stoichiometric flame conditions. The SBNR of RST was estimated at room temperature air condition. The SBNR of RST in room temperature air is higher than in flames due to higher number density. The imaging spatial resolution is better than 70×70 μm^2 (for ~23×23 mm^2 imaging size) and the thickness of the combined laser sheet was measured to be 100 μm. The spatial resolution has been discussed in [10]

where it was defined from the finest resolvable pattern on a resolution target (USAF-1951). This estimated spatial resolution is about 3 times as much as the projected pixel size (which is about 24 μm). Special attention has been paid to the CH detection as CH is the key radical for determining distributed reactions; the CH LIF emission spectra were examined in both laminar and turbulent flames to ensure interference-free detection. Furthermore, additional supports for a high-quality and high-fidelity CH measurement as reported in our previous study [10] are as follows: (1) HCO-PLIF (another reaction zone marker [3]) exhibited similar distributed features to that of the CH-PLIF; (2) CH-PLIF images exhibit clearly spatial correlations as well as (anti-) correlation of signal intensities at both large and small scales with other scalars (e.g. CH_2O and OH) that were measured simultaneously with CH using independent detection system.

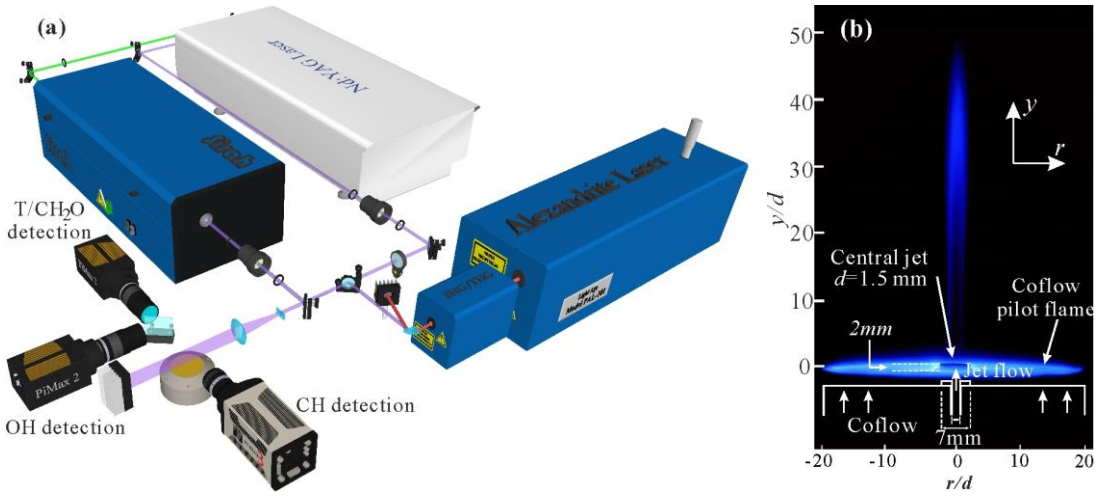

Figure 1. (a) Experimental setup for simultaneous T/CH/OH imaging measurements, and (b) schematic plot of the burner with photograph of a flame.

As shown in Fig. 1b, the burner is made up of a porous-plug laminar flame burner (61 mm in diameter) and a central jet of 1.5 mm in diameter (*d*). The jet is made of a stainless tube of thickness

2 mm and an outer diameter of 7 mm to prevent direct mixing between the jet and the coflow at the jet exit. A flat laminar CH_4/air flame with the exit reactant flow velocity of 0.3 m/s at 300 K and equivalence ratio Φ=0.9 was stabilized on the porous-plug burner, providing a hot environment to sustain the central jet methane/air flames. The coflow condition was deliberately kept the same to ensure the same ambient environment for all jet flames studied. The jet inlet velocity (U_0) was varied systematically from 11 to 418 m/s (U_0 is the bulk flow velocity at the nozzle exit, i.e., the volume flow rate divided by the section area of the nozzle). Equivalence ratio, Φ, was varied from 0.4 to 1 to cover a wide range of flames residing in both the laminar flame regime and the turbulent TRZ/DRZ regimes. The characteristic quantities of the investigated flames are summarized in Table 1. The flames were referred to as Lund University Piloted Jet (LUPJ) premixed flames and labeled as LUPJα-β, where α and β represent the values of Φ and U_0 of the flames, respectively.

The laminar flame speed (S_L) at different Φ given in Table 1 was determined experimentally using the relation $S_L=U_0\times\sin\theta$, where θ is the half angle of the flame cone determined from the inner boundary of the OH-PLIF field of a laminar flame at a jet velocity of 11 m/s. At this speed, the OH/CH_2O/CH layers are smooth and of perfectly conical shape. The difference of using the OH, CH_2O or CH layer to determine θ is small since the CH and CH_2O layers are thin and coincide with the inner boundary of the OH layer [11]. The laminar flame thickness δ_L is defined as $\delta_L = \frac{T_p - T_u}{|\nabla T|_{max}}$ where the temperature of products (T_p), unburnt reactants (T_u) and the maximum temperature gradient $|\nabla T|_{max}$ were measured using RST in the corresponding laminar flames. The value of S_L for the stoichiometric laminar flame (LUPJ10-11) determined from experiment is about 10% higher than the value reported in the literature. This is due to the back-support from the pilot flame, which is clearly evidenced by the fact that the laminar flame Φ=0.4 is below the lean flammability limit while

with the back-support of the pilot flame the value of S_L for Φ=0.4 is 21.4 cm/s. For the stoichiometric flame the back-support plays a less important role. The use of experimentally determined S_L and δ_L is to enable consistently scaling the turbulent statistical quantities for all range of Φ and to account for the effects of the pilot flame and burner configuration [11].

For the studied turbulent flames listed in Table 1, the characteristic integral length scale (l_0) and the turbulent intensity (u') were determined at axial location y/d=30 from laser Doppler anemometry (LDA) measurements [11] which showed that both l_0 and u' have rather minor dependence on Φ. From the LDA data of the current flame series presented in [11] it is seen that, for the flame height y/d ~15 to 40, the variation of u' is not significant. As shown later the reaction zone and preheat zone in these flames are within y/d<32. Thus, the LDA data at y/d=30 characterize reasonably well the mean turbulent data in the flame. Following the formulations of Peters [1] as given in the footnotes of Table 1, the jet/turbulent Reynolds number (Re_{jet}/Re_t), the Kolmogorov length scale (η) and the Karlovitz number (Ka) for the investigated flames were estimated.

Table 1.

Experimental cases and key parameters. The laminar flame speed (S_L) and thermal thickness (δ_L) are determined based on the measurement on LUPJ flames at jet velocity of 11 m/s [11]. [a)] Jet Reynolds number, $Re_{jet}=U_0d/\nu$ (ν is the kinematic viscosity of the reactant mixture at 298 K); [b)] Turbulent Reynolds number, $Re_t=(u'l_0)/(S_L\delta_L)$; [c)] Kolmogorov length scale, $\eta=l_0Re_t^{-3/4}$; [d)] Karlovitz number: $Ka=(u'/S_L)^{3/2}\times(\delta_L/l_0)^{1/2}$.

Flame cases	Φ	S_L (cm/s)	δ_L (mm)	U_0 (m/s)	Re_{jet} [a]	Re_t [b]	l_0 (mm)	η [c] (μm)	u'/S_L	l_0/δ_L	Ka [d]
LUPJ10-66	1.0	42.5	0.48	66	6306	95	2.9	96	16	6.0	25
LUPJ07-66	0.7	33.2	0.60			97		95	20	4.8	40
LUPJ06-66	0.6	31.5	0.62			99		93	21	4.7	44
LUPJ04-66	0.4	21.4	0.85			107		89	31	3.4	92
LUPJ10-110	1.0	42.5	0.48	110	10510	190		57	31	6.0	70
LUPJ07-110	0.7	33.2	0.60			195		56	40	4.8	113
LUPJ06-110	0.6	31.5	0.62			199		56	42	4.7	125
LUPJ04-110	0.4	21.4	0.85			214		53	62	3.4	261

LUPJ10-165	1.0	42.5	0.48	165	15764	238	49	39	6.0	98
LUPJ07-165	0.7	33.2	0.60			244	48	50	4.8	158
LUPJ06-165	0.6	31.5	0.62			248	47	52	4.7	174
LUPJ04-165	0.4	21.4	0.85			267	45	77	3.4	365
LUPJ10-220	1.0	42.5	0.48	220	21019	317	39	52	6.0	151
LUPJ07-220	0.7	33.2	0.60			325	38	66	4.8	244
LUPJ06-220	0.6	31.5	0.62			331	38	70	4.7	268
LUPJ04-220	0.4	21.4	0.85			356	36	103	3.4	561
LUPJ10-330	1.0	42.5	0.48	330	31529	476	26	78	6.0	277
LUPJ07-330	0.7	33.2	0.60			487	26	99	4.8	448
LUPJ06-330	0.6	31.5	0.62			496	26	105	4.7	496
LUPJ04-330	0.4	21.4	0.85			534	24	154	3.4	1031
LUPJ10-418	1.0	42.5	0.48	418	39936	603	22	98	6.0	394
LUPJ07-418	0.7	33.2	0.60			617	21	126	4.8	639
LUPJ06-418	0.6	31.5	0.62			629	21	133	4.7	707
LUPJ04-418	0.4	21.4	0.85			676	20	196	3.4	1470

3. Results and discussion

3.1 Flame structure

Figure 2 shows instantaneous multi-scalar images acquired in the LUPJ flames of U_0=165 m/s for equivalence ratios Φ=1.0 and 0.6. For illustration, the CH and OH images were normalized by their maximal intensities. The broadened/distributed CH layer in both flames can clearly be observed. It can be seen that distributed CH appears more prominently in the low-temperature regions; however, there are regions where CH signals are found at high intensity along with high temperature and rather high OH signals, as indicated by the windows marked with the dashed boxes. The arrows in Fig. 2 mark regions where both the CH and T are low.

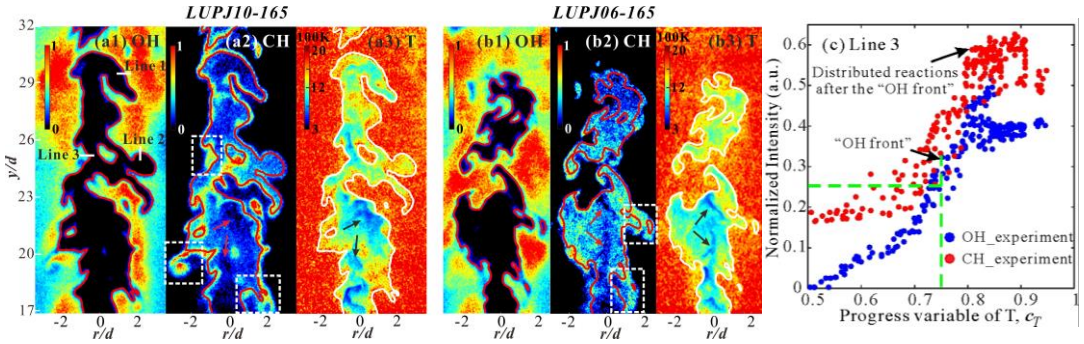

Figure 2. Simultaneous T/CH/OH image for the flames (a1-a3) LUPJ10-165 and (b1-b3) LUPJ06-165, and (c) intensities of OH- and CH-PLIF vs. normalized temperature sampled along line-3 indicated in (a1). The iso-surface of 25% of OH PLIF intensity was superimposed onto the images. Dashed boxes highlight the presence of CH signals at high-temperature regions.

DNS studies [18,19] indicated that distributed reactions in high Ka flames are facilitated by the turbulent transport of radicals, e.g., H and OH, from the high-temperature region to the low-temperature region where radical recombination reactions can take place. As seen in Fig. 2, although regions of high OH signals are frequently associated with high temperatures, there are OH signals in low-temperature regions. Note that in Fig.2 OH intensity lower than 25% of its maximum (as separated by the red iso-lines) is not visible due to the choice of color scale. Fig. 2c shows the normalized OH and CH PLIF intensities along line-3 in Fig.2a, as a function of the local normalized temperature $c_T=\frac{T-T_u}{T_p-T_u}$. T_p is set to the measured mean temperature of the coflow flame (1850K) and T_u =300K. It is shown that both OH and CH PLIF signals can appear simultaneously over a wide range of c_T values ($0.5<c_T<0.9$). The intensities of both OH and CH PLIF increase with temperature.

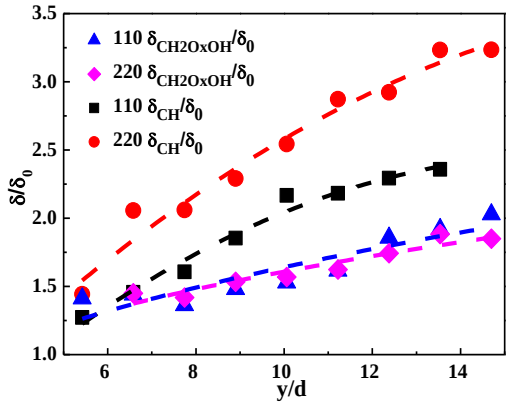

Figure 3. Mean thickness of CH layer and the overlapping layer of OH and CH_2O along the flame height for two flames, LUPJ10-110 and LUPJ10-220.

The broadening of CH layers can be compared with the layer of the "heat release marker", i.e., the overlapping region of OH-PLIF and CH_2O-PLIF. Figure 3 shows the statistical mean thickness of the CH layer and the overlapping region of OH and CH_2O along the flame height for two LUPJ10 flame cases. The mean thickness of these layers is computed at a given flame height for each PLIF image and then ensemble-averaged using about 300 images. The image processing included background subtraction, energy distribution correction of laser beam profile and usage of a 2 x 2 pixels median filter to reduce noise (cf. [10]). Each pixel in the PLIF images was then normalized by the maximum signal intensity. The values below 0.01 and above 0.99 were set to 0 and 1, respectively. After that, the PLIF images were binarized with a threshold just above the noise level. Then, the thickness of CH was calculated by counting the number of pixels at the flame height which was converted into length scale afterwards.

The thickness of the layers shown in Fig. 3 has been normalized with the corresponding thickness of the laminar flame of U_0=11 m/s. The thickness of the CH layer increases with flame height as well as with U_0 (thus Ka). Within the range of flame height shown in the figure, the CH

layer of the LUPJ10-220 flame is broadened to about 3 times of that of the laminar flame. On the contrary, the broadening of the overlapping layer of OH and CH_2O is not sensitive to U_0 (thus Ka), and the mean thickness of this 'heat release' layer is considerably thinner than the CH layer.

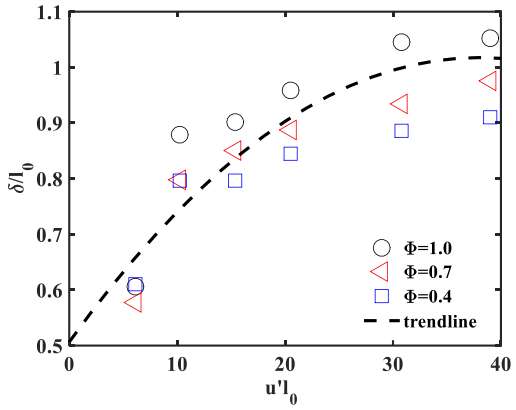

Figure 4. Thickness of the CH_2O layer at y/d=10 for the flames listed in Table 1. l_0 is the integral length scale at y/d=10, determined from the LDA experiments [11].

The CH_2O layer may be used as the preheat zone marker [20]. Figure 4 shows that the statistical mean thickness of the CH_2O layer at $y/d = 10$ increases with $u'l_0$ (thus with U_0 and Ka). The mean thickness was computed in a similar way as that of CH layer. All flames show a significant broadening of the CH_2O layer in comparison with the laminar flames ($u' = 0$) at the corresponding equivalence ratio. The broadening increases along the flame height (for brevity the figure is not shown here). The increase of the mean thickness of the CH_2O layer with U_0 and Ka may be explained as follows: as the jet velocity increases, the turbulent eddy diffusivity ($u'l_0$) increases, which in turn leads to the increase of eddy transfer in the preheat zone. It is interesting to note that at high jet velocity, the broadening of the preheat zone saturates to the level of integral length. The preheat zone appears not to be thicker than the integral eddies.

3.2 Turbulent burning velocity

Turbulent burning velocity can be defined in different ways, for example, a global consumption speed of the flame ($S_{T,c}$) can be defined as [15,6],

$$S_{T,c} = \dot{m}_{in}/(\rho_u \bar{A}_f), \quad (1)$$

where $\dot{m}_{in}$ is the mass flow rate of the jet, ρ_u is the density of the unburned mixture, and $\bar{A}_f$ is the characteristic area of the mean flame front. Alternatively, an area-averaged local displacement speed on a given surface of the mean flame can be defined as,

$$S_{T,d} = \int s_d dA \,/\bar{A}_f, \quad (2)$$

where s_d is the local displacement speed on the given surface and $\bar{A}_f$ is the total area of the surface. Integration of Eq. (2) is done for the entire surface. For a statistical stationary flame the local displacement speed on a surface of the mean flame is equal to the local mean flow velocity normal to surface, v_n, owing to the mass conservation law. It can be shown that $S_{T,d} = \frac{\int s_d dA}{\bar{A}_f} = \frac{\rho \int v_n dA}{\rho \bar{A}_f} = \dot{m}_{in}/(\rho \bar{A}_f) = S_{T,c}\theta$, where ρ is the mean density on the given surface and $\theta = \rho_u/\rho$ is the ratio of density of the unburned mixture to the density on the given surface, which is proportional to the ratio of the temperature on the surface to that of the unburned mixture. The calculation of $S_{T,d}$ requires information on the mean flow velocity on the flame surface and information on the mean flame surface position, whereas $S_{T,c}$ only requires the information on the mean flame surface position and the mass flow rate of the jet.

It is clear that $S_{T,d}$ and $S_{T,c}$ are equal if the mean flame surface in Eqs. (1) and (2) is defined in the preheat zone where $\theta = \rho_u/\rho \sim 1$. In a one-dimensional unstretched laminar flame, the

laminar flame speed S_L is defined as the displacement speed in the beginning of the preheat zone. Following the same analogy, the turbulent burning velocity should also be defined at the beginning of the preheat zone. A convenient choice is to use the temperature field, i.e., small value of c_T (e.g. 0.1) to compute the mean flame surface area for Eq. (1). Equivalently, one can use the mean reaction progress variable defined based on the mean CH_2O field. Experimental data of $S_{T,c}$ reported in the literature are often based on the mean flame surface area defined at the OH layer [4]. For statistically planar flames, the mean surface area defined in different layers of the flame is the same; thus, $S_{T,c}$ determined using different layers is identical. For jet flames the situation is very different. In the TRZ and DRZ regimes the preheat zone is thickened by turbulence, in particular at the flame tip. This will make the mean flame surface area defined in the OH layer much larger than that defined in the CH_2O layer, which will result in an underestimated $S_{T,c}$.

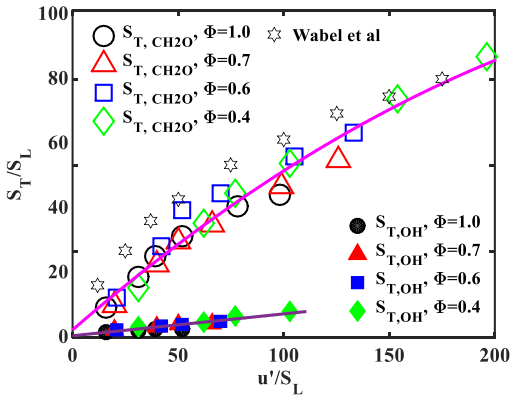

Figure 5. Turbulent burning velocity normalized with the corresponding laminar flame speed ($S_{T,c}/S_L$) as a function of turbulent intensity, u'/S_L, for a series of the turbulent flames listed in Table 1. Two mean flame surface areas are used, a CH_2O based reaction progress variable $c_{CH2O} = 0.5$, and a OH based reaction progress variable $c_{OH} = 0.2$. The data of Wabel et al. [6] are also shown for comparison.

The OH and CH_2O layers are used to determine the mean flame surface. Due to the use of the large pilot flame the instantaneous iso-surfaces of the OH and CH_2O layers are continuous. This allows one to determine turbulent burning velocity using these species. To compute the mean flame area, reaction progress variables were calculated based on binarized OH and CH_2O PLIF images. These were obtained in a similar way as the aforementioned procedure of post-processing for CH_2O/CH layer thickness, where a threshold which is about 0.3 was chosen to binarize the PLIF images at the leading edge of the preheat zone [6, 7]. In addition, canny edge detection was used to find the interface between fuel zone and preheat zone in the binary image. The area inside the interface represents unburnt region while burnt region (starts from forming CH_2O) is outside the interface. Namely, binary value in the unburnt region is 0 and that is 1 in the burnt region. Finally, about 300 binary images were lumped together to have an ensemble-averaged results, i.e. the mean progress variables based on OH and CH_2O.

Figure 5 shows the global consumption speed determined from both the CH_2O layer and the OH layer, for the various flames listed in Table 1. It is seen that $S_{T,c}$ defined using $c_{\mathrm{CH2O}} = 0.5$ is about 4-6 times of that determined using $c_{\mathrm{OH}} = 0.2$. The results are compared with the experimental data of Wabel et al. [6], obtained at high turbulent intensity, u'/S_L up to 160. $S_{T,c}$ reported by Wabel et al. [6] was determined using Eq. (1) with the mean area defined at $c_{\mathrm{OH}} = 0.2$ and $c_{\mathrm{OH}} = 0.5$. They reported a difference of $S_{T,c}$ computed using the two iso-surfaces by a factor 2, indicating the relative lower sensitivity of $S_{T,c}$ to the definition of the mean surface area than the present flames. It is worth noting that the flame in Wabel et al. [6] is much shorter than the present flames and the jet has a much larger diameter, about 10 times of that of the current flames. This

makes the area defined in different layers of the flames of Wabel et al. [6] less sensitive to the definition of the mean flame surface.

The turbulent burning velocity in the present series of flames determined using $c_{\mathrm{CH2O}} = 0.5$ is consistent with the data of Wabel et al. [6]. It is expected that $S_{T,c}$ of Wabel et al. would be higher than the present data at a given u'/S_L, if it were evaluated at $c_{\mathrm{CH2O}} = 0.5$. This difference is expectable and it is attributed to the difference of jet diameter and integral length scales. Despite the differences, the present data shows a similar trend of the turbulent burning velocity in the TRZ and DRZ regimes as that of Wabel et al. [6]; $S_{T,c}$ increases monotonically with the turbulent intensity, first linearly until $u'/S_L \sim 40$, and then it increases at a slower rate, which is known as the bending of turbulent burning velocity at high turbulent intensities [1]. Similar to the results of Wabel et al. [6], there is no 'flatten-out' tendency of $S_{T,c}$ within the present range of turbulence intensity. $S_{T,c}$ from all four equivalence ratios and jet velocities falls nicely into a non-dimensional profile of $S_{T,c}/S_L$ as a function of u'/S_L.

In the laminar flamelet regime the increase of $S_{T,c}/S_L$ is proportional to the wrinkle ratio of area (a ratio of the wrinkled turbulent flame surface area to that of the mean flame surface area) [14]. Figure 6 shows the winkled area ratio determined in the CH_2O and OH layers. Since the PLIF imaging is limited to two-dimensional (2D) information, only 2D wrinkle ratio is computed, which is known to be smaller than the 3D wrinkle ratio. The wrinkle ratio in both the OH layer and the CH_2O layer is about 1.3 – 1.5, which is significantly smaller than the value of $S_{T,c}/S_L$. Similar results are reported in the work of Wabel et al. [6] at high Ka conditions. It is likely due to the small integral scale in the present experiment. Wrinkling is more effective for eddies larger than the thickness of the flame. With a larger integral length, a larger spectrum range of eddies could wrinkle the flame,

resulting in a larger wrinkle ratio [21].

One may speculate that the low wrinkle ratio is partly due to the low PLIF resolution. In Fig. 6 the wrinkle ratios obtained with two different OH-PLIF image resolutions are compared. Clearly, with higher resolution the wrinkle ratio is larger. Nevertheless, the wrinkle ratio is by far smaller than the value of $S_{T,c}/S_L$, and the winkle ratio flattens out at high u'/S_L, which is different from the profile of $S_{T,c}/S_L$. The implication of the small wrinkle ratio in comparison to $S_{T,c}/S_L$ is that the propagation of the present high Ka flames is not by area wrinkling, rather it is attributed to the turbulent heat and mass transfer in the broadened preheat and reaction zones.

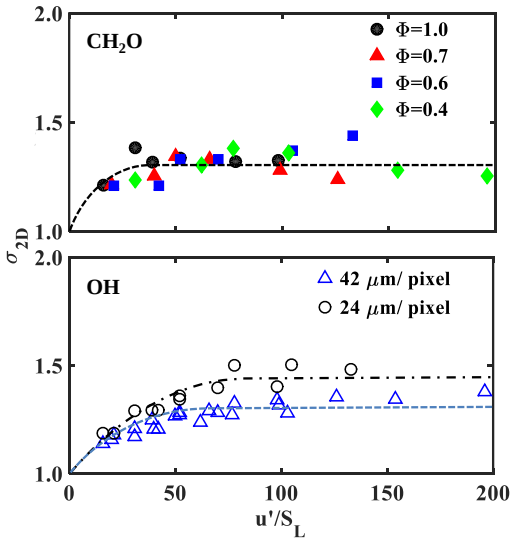

Figure 6. Two-dimensional flame surface wrinkle ratios computed from $c_{\mathrm{CH2O}} = 0.5$ and $c_{\mathrm{OH}} = 0.2$ for different flame conditions (Φ=0.4-1.0) with the 42 μm/pixel resolution, and from $c_{\mathrm{OH}} = 0.2$ with the 24 μm/pixel resolution for the flames with Φ=0.6.

4. Concluding remarks

A series of turbulent methane/air premixed jet flames with different jet speeds and equivalence ratios

were studied using simultaneous OH/CH/T and CH/OH/CH_2O planar imaging measurements. Simultaneous OH/CH/T measurements directly correlate the temperature with CH-PLIF and OH-PLIF. It was found that CH and OH PLIF overlap in a wide range of temperature at high Karlovitz number conditions. The reaction zone characterized using CH-PLIF signal shows increased broadening with increasing jet velocity or Karlovitz number. The heat release zone characterized by the overlapping region of OH-PLIF and CH_2O-PLIF is however not as significantly broadened as the CH layer. The broadening of this heat release rate is not sensitive to the jet velocity. The preheat zone characterized with the CH_2O-PLIF signal shows increased broadening with increasing turbulent eddy viscosity ($u'l_0$). The broadening of this layer at high Ka flames is on the order of the turbulent integral length scale. The turbulent burning velocity is shown to increase monotonically with the turbulence intensity (u'/S_L). At very high turbulent intensity, $u'/S_L \sim 200$, the turbulent burning velocity is about 80 times of that of the corresponding laminar flame. In the thin-reaction zone and distributed reaction zone regimes, the governing mechanism of enhanced flame propagation is the turbulent eddy transfer of heat and mass in the preheat zone and reaction zone, while the contribution of flame front wrinkling to the turbulent burning velocity is rather minor.

Acknowledgements

The financial support comes from VR (Swedish Research Council), CECOST and the European Research Council Advanced Grant.

References

[1] N. Peters, Turbulent Combustion, Cambridge University Press, Cambridge, 2000.

[2] L.P.H. de Goey, T. Plessing, R.T.E. Hermanns, N. Peters, Proc. Combust. Inst. 30 (2005)

859-866.

[3] B. Zhou, J. Kiefer, J. Zetterberg, Z.S. Li, M. Alden, Combust. Flame 161 (2014) 1566-1574.

[4] J.F. Driscoll, Prog. Energy Combust. Sci. 34 (2008) 91-134.

[5] P.H. Paul, H.N. Najm, Symp. (Int.) Combust. 27 (1998) 43-50.

[6] T. M. Wabel, A. W. Skiba, J. F. Driscoll, Proc. Combust. Inst. 36 (2017) 1801-1808.

[7] T. M. Wabel, A. W. Skiba, J. E. Temme, J. F. Driscoll, Proc. Combust. Inst. 36 (2017) 1809-1816.

[8] A. W. Skiba, T. M. Wabel, C. D. Cater, S. D. Hammack, J. E. Temme, L. Tonghun, J. F. Driscoll, Proc. Combust. Inst. 36 (2017) 4593-4601.

[9] T. M. Wabel, A. W. Skiba, J. F. Driscoll, Combust. Flame 188 (2017) 13-27.

[10] B. Zhou, C. Brackmann, Z.S. Li, M. Alden, X.-S. Bai, Proc. Combust. Inst. 35 (2015) 1409-1416.

[11] B. Zhou, C. Brackmann, Q. Li, Z. Wang, P. Petersoon, Z. Li, M. Alden, X.-S. Bai, Combust. Flame 162 (2015) 2937-2953.

[12] B. Zhou, Q. Li, Y. He, P. Pertersson, ZS.Li, M. Alden, X.S. Bai, Combust. Flame 162 (2015) 2954-2958.

[13] D. Bradley, Proceedings of the Combustion Institute 24 (1992).

[14] G. Damkohler, Z Elktrochem Angew P 46 (1940) 601-626.

[15] S.A. Filatyev, J.F. Driscoll, C.D. Carter, J.M. Donbar, Combust. Flame 141 (2005) 1-21.

[16] A.Y. Poludnenko, E.S. Oran, Combust. Flame 158 (2011) 301-326.

[17] J.B. Bell, M.S. Day, J.F. Grcar, Proc. Combust. Inst. 29 (2002) 1987-1993.

[18] A.J. Aspden, M.S. Day, J.B. Bell, Proc. Combust. Inst. 35 (2014) 1321-1329.

[19] H. Carlsson, R.X. Yu, X.S. Bai, Int. J. Hydrogen Energy 39 (2014) 20216-20232.

[20] Z.S. Li, B. Li, Z.W. Sun, et al., Combust. Flame 157 (2010) 1087–1096.

[21] H. Kolla, J. W. Rogerson, N. Swaminathan, Combust. Sci. Technol. 182 (2010) 284-308.